J|A|C|S COMMUNICATIONS

Published on Web 09/24/2010

High-Yield Synthesis of Ultralong and Ultrathin Zn_2GeO_4 Nanoribbons toward Improved Photocatalytic Reduction of CO_2 into Renewable Hydrocarbon Fuel

Qi Liu,[†,§,⊥] Yong Zhou,*[,†,‡,∥] Jiahui Kou,[†,∥] Xiaoyu Chen,[†,§] Zhongping Tian,[†,‡] Jun Gao,[†,‡] Shicheng Yan,[†,‡,∥] and Zhigang Zou*[,†,‡,§,∥]

Eco-materials and Renewable Energy Research Center (ERERC), School of Physics, Department of Materials Science and Engineering, and National Laboratory of Solid State Microstructures, Nanjing University, Nanjing 210093, P. R. China, and School of Mechanical and Automotive Engineering, Anhui Polytechnic University, Wuhu 241000, P. R. China

Received August 4, 2010; E-mail: zhouyong1999@nju.edu.cn; zgzou@nju.edu.cn

Abstract: Single-crystalline Zn_2GeO_4 nanobelts with lengths of hundreds of micrometers, thicknesses as small as ~7 nm, and aspect ratios of up to 10 000 were synthesized in a binary ethylenediamine/water solvent system using a solvothermal route. The ultralong and ultrathin geometry of the Zn_2GeO_4 nanoribbon proves to greatly promote the photocatalytic activity toward reduction of CO_2 into renewable hydrocarbon fuel (CH_4) in the presence of water vapor.

Studies of 1D ternary nanostructures, in comparison with 1D binary ones, are relatively more meaningful because the ternary nanostructures exhibit not only more complex functions but also properties that are readily tunable by changing the ratio of the component elements.[1−3] Reports of 1D ternary nanostructures, specifically nanoribbons, however, have been limited because of the considerable difficulty of their synthesis.

Zinc orthogermanate (Zn_2GeO_4) is an important ternary oxide that exhibits negative thermal expansion below ambient temperature.[4] It also exhibits high-wavelength selectivity in UV photodetectors with fast response and recovery time,[5] bright white-bluish luminescence,[6] photocatalytic water splitting, and mineralization of volatile aromatic hydrocarbons.[7] Several solution routes and gas-phase evaporation techniques have been developed for the preparation of 1D nanorods[7c,d,8] and nanowires of Zn_2GeO_4.[5]

Herein we report for the first time the high-yield synthesis of single-crystalline Zn_2GeO_4 nanobelts with lengths of hundreds of micrometers, thickness as small as ~7 nm (corresponding to five repeating cell units), and aspect ratios of up to 10 000 in a binary ethylenediamine (En)/water solvent system using a solvothermal route. The ultralong and ultrathin geometry of the Zn_2GeO_4 nanoribbon greatly improves the photocatalytic activity toward reduction of CO_2 into renewable hydrocarbon fuel (CH_4) in the presence of water vapor.

The preparation procedure is described in the Supporting Information (SI). All of the X-ray diffraction (XRD) peaks for the Zn_2GeO_4 nanobelt can be assigned to the rhombohedral phase of Zn_2GeO_4 (JCPDS no. 11-0687) with lattice constants $a = b = 1.423$ nm, $c = 0.953$ nm, $\alpha = \beta = 90°$, and $\gamma = 120°$ (Figure SI1). No impurity phases such as ZnO and GeO_2, which appear in other solution methods,[7a] were detected. The small-angle XRD pattern showed no detectable diffraction peaks in the low-angle range, indicating a pure inorganic phase rather than an inorganic−En hybrid.[9,10] Thermogravimetric (TG) analysis also confirmed that no significant decomposition occurred, and weight loss of only 2.5% was observed after heating to 500 °C (Figure SI2), which was assignable to desorption of surface-absorbed En and H_2O from the nanoribbon.

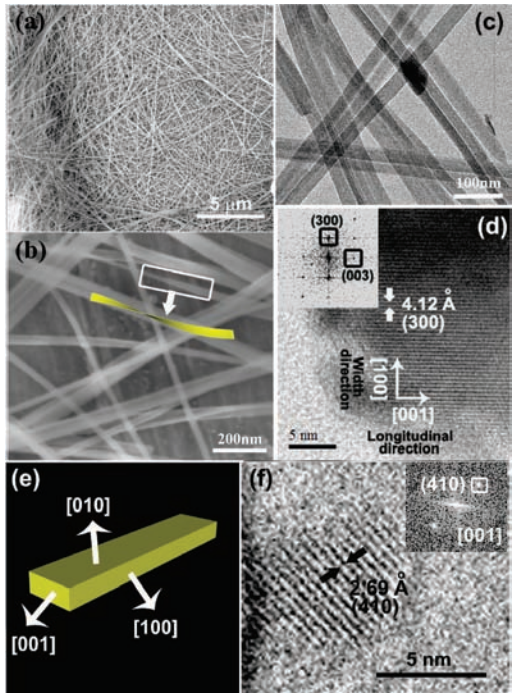

Figure 1. (a, b) FE-SEM, (c) TEM, and (d) HRTEM images of the Zn_2GeO_4 nanoribbons. The inset of (d) shows the FFT pattern obtained from the HRTEM image. (e) Structural model of a nanoribbon. (f) HRTEM image taken along [001].

Field-emission scanning electron microscopy (FE-SEM) images show elegant, flexible, ultralong nanobelts (Figure SI3). The lengths of hundreds of micrometers facilitated connection of the nanoribbons to electrodes for detection of their optoelectronic properties, which is currently underway. The uniform width of 20−50 nm over their entire length resulted in an aspect ratio (length to width) of up to 10 000 (Figure 1a,b). A specifically twisting ribbon is schematically illustrated in Figure 1b.

Transmission electron microscopy (TEM) images further demonstrate the ribbonlike architecture with light contrast (Figure 1c). The high-resolution TEM (HRTEM) image (Figure 1d) shows that the interplanar *d* spacing of ~0.412 nm corresponds to the (300)

[†] ERERC, Nanjing University.
[‡] School of Physics, Nanjing University.
[§] Department of Materials Science and Engineering, Nanjing University.
[∥] National Laboratory of Solid State Microstructures, Nanjing University.
[⊥] Anhui Polytechnic University.

lattice planes of an orthorhombic Zn_2GeO_4 phase. The fast Fourier transform (FFT) pattern indicates that the nanoribbon is a uniform single crystal with the longitudinal direction along [001] and the width direction along [100] (Figure 1e). The two major exposed surfaces of the nanobelts were determined to be {010} facets. Figure 1f presents a typical HRTEM image taken along [001], from which the thickness of the nanoribbon was measured to be ~7 nm. The AFM image of the nanoribbon (Figure SI4) also reveals the thickness to be ~7 nm, corresponding well to five repeating cell units (i.e., 5×1.423 nm $= 7.115$ nm). A crystalline model of the nanoribbon can thus be schematically illustrated as shown in Figure SI5. The precedent cetyltrimethylammonium bromide (CTAB)-assisted Zn_2GeO_4 nanorods[7c,d] and Zn_2GeO_4 nanowires obtained by Au-catalyzed vapor−liquid−solid synthesis show a mainly dominant growth direction along [110],[5] indicating that the present Zn_2GeO_4 nanoribbons were produced by a totally different growth mechanism than the others.

It is well-known that alkylamines display bifunctionalities that mediate the crystal structure growth and control the 1D morphology of II−VI semiconductor and inorganic−organic hybrids because they can adsorb on solid surfaces and selectively bind to some specific panels to control the velocity and direction of crystal growth; this has been called the solvent-coordination molecular-template mechanism.[9−12] In the present system, employment of pure En as a single solvent produced small Zn_2GeO_4 nanorods with lengths of 200 nm and diameters of 5 nm growing along the [001] direction (Figure SI6). Use of pure water as the solvent enabled us to obtain a mixture of microscale rods and particles (Figure SI7). As a result, we believe that the nanoribbons formed in the En/H_2O binary solvent mainly originate from the structure-directing and regulating role of En through coordination and H-bonding interactions between the amino groups of En and the surface Zn, Ge, and O moieties of the Zn_2GeO_4 framework. The presence of H_2O may partially protonate En molecules, which may weaken and mediate the interaction of En with the inorganic framework, thereby allowing the initially formed nanorod to continue to grow, specifically along the [001] direction. While H_2O/alkylamine mixed-solvent systems were developed early for the synthesis of binary inorganic and hybrid nanostructures,[9a,b] the novelty of our work is to extend this system to the successful one-step synthesis of ultralong ternary oxide nanoribbons.

Reduction of CO_2 to valuable hydrocarbons using solar energy is one of the best solutions to both the global warming and the energy shortage problems. Generally, CO_2 in the presence of water vapor can be photoreduced to CH_4 using a wide-band-gap semiconductor such as TiO_2 as a photocatalyst.[13] Here we performed photocatalysis of the CO_2 + gaseous H_2O reaction in a gas−solid system over the Zn_2GeO_4 nanoribbon. The photogenerated holes in the valence band oxidize water to generate hydrogen ions via the half-reaction $H_2O \rightarrow {}^1/_2O_2 + 2H^+ + 2e^-$ ($E^\circ_{ox} = 0.82$ V vs NHE), and the photogenerated electrons in the conduction band reduce CO_2 to CH_4 via the reaction of $CO_2 + 8e^- + 8H^+ \rightarrow CH_4 + 2H_2O$ ($E^\circ_{red} = -0.24$ V vs NHE). Investigation of the electronic structure of a Zn_2GeO_4 nanoribbon using density functional theory demonstrated that the lower part of the valence band consists of the Zn 3d and O 2p orbitals, whereas the upper part is composed of the O 2p orbitals. The bottom of the conduction band is composed of the Ge 4p orbitals with small contributions from the Zn 4s and 4p orbitals.[7b] The band gap of the as-prepared Zn_2GeO_4 nanoribbon was determined to be ~4.5 eV on the basis of the UV−vis absorption spectrum (Figure SI8). The position of the conduction band of the as-prepared Zn_2GeO_4 nanoribbons could be determined using the equation $E_{CB} = X - E_c - 0.5E_g$, where E_c is the energy

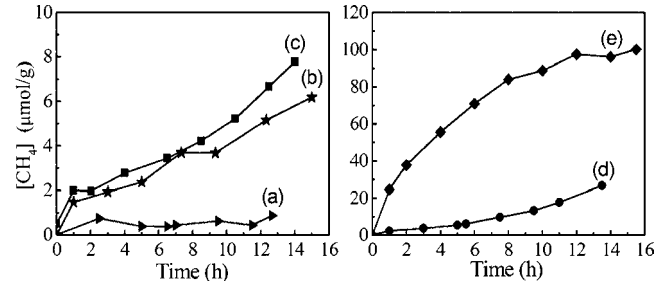

Figure 2. CH_4 generation over (a) the SSR sample, (b) nanoribbons, (c) 1 wt % Pt-loaded nanoribbons, (d) 1 wt % RuO_2-loaded nanoribbons, and (e) 1 wt % RuO_2 + 1 wt % Pt-coloaded nanoribbons as a function of light irradiation time.

of free electrons on the hydrogen scale (4.5 eV), X is the electronegativity of the semiconductor, and E_g is the band-gap energy of the semiconductor. The edge of the valence band (E_{VB}) of Zn_2GeO_4 was determined to be 3.8 V (vs NHE) more positive than $E^\circ(H_2O/H^+)$ (0.82 V vs NHE), and the edge of the conduction band was estimated to be −0.7 V (vs NHE), which is more negative than $E^\circ(CO_2/CH_4)$ (−0.24 V vs NHE). This indicates that the photogenerated electrons and holes in the irradiated Zn_2GeO_4 can react with adsorbed CO_2 and H_2O to produce CH_4, as described in following equation:

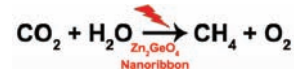

Figure 2 shows that the Zn_2GeO_4 nanoribbons rendered a CH_4 yield of ~1.5 μmol g^{-1} during the first hour under light illumination (curve b). A CO_2 reduction experiment performed in the dark or in the absence of the photocatalyst showed no appearance of CH_4, proving that the CO_2 reduction reaction is driven by light with the photocatalyst. Bulk Zn_2GeO_2 obtained by conventional solid-state reaction (SSR) at 1200 °C for 16 h produced a trace amount of CH_4 (curve a). The higher photocatalytic activity of the Zn_2GeO_4 nanoribbons toward reduction of CO_2 relative to that of the SSR sample can be attributed to the following four reasons: (1) Reducing the lateral dimension to the nanometer length scale as in the nanobelts offers a high specific surface area of 28.27 m^2/g, which is >37 times larger than the area of 0.75 m^2/g for the SSR material. (2) The superb crystal quality excludes the possibility of any grain boundaries and/or other interfaces (which usually act as recombination sites in polycrystalline materials). This should favor improved separation of the photogenerated electron and hole and decrease the electron−hole recombination rate. (3) The ultralong longitudinal dimension provides a sufficiently spacious transport channel for charge separation. (4) The ultrathin geometry of the nanoribbons allows charge carriers to move rapidly from the interior to the surface to participate in the photoreduction reaction. The rate of CH_4 generation over the Zn_2GeO_4 nanoribbon could be significantly enhanced by loading of Pt (curve c) or RuO_2 (curve d) and especially by coloading of Pt and RuO_2 (curve e; 25 μmol g^{-1} during the first hour) as a cocatalyst (see Figure SI9) to improve the separation of the photogenerated electron−hole pairs, as demonstrated in photocatalytic water splitting.[7]

In summary, ultralong, ultrathin, high-aspect-ratio single-crystalline Zn_2GeO_4 nanobelts have been synthesized in an En/H_2O binary solvent system, and they exhibit promising photocatalytic activity for reduction of CO_2 to CH_4. This binary solvent system may provide a new route for preparing other 1D ternary oxides.

Acknowledgment. Financial support from the National Basic Research Program of China (973 Program, 2007CB613305), JST-

MOST (No. 2009DFA61090), JSPS-NSFC (No. 20811140087), and NSFC (No. 50732004 and 20971048) are gratefully acknowledged.

Supporting Information Available: Experimental details; XRD pattern; TG curve; FE-SEM, AFM, and HRTEM images; and UV−vis absorption spectrum. This material is available free of charge via the Internet at http://pubs.acs.org.

References

(1) Xia, Y. N.; Yang, P. D.; Sun, Y. G.; Wu, Y. Y.; Mayers, B.; Gates, B.; Yin, Y. D.; Kim, F.; Yan, Y. Q. *Adv. Mater.* **2003**, *15*, 353.
(2) (a) Zhou, Y.; Kogiso, M.; Shimizu, T. *J. Am. Chem. Soc.* **2009**, *131*, 2456. (b) Zhou, Y. *Curr. Nanosci.* **2006**, *2*, 123.
(3) Sun, Y. G.; Hu, J. Q.; Chen, Z. G.; Bando, Y.; Golberg, D. *J. Mater. Chem.* **2009**, *19*, 7592.
(4) Steven, R.; Woodfield, B. F.; Boerio-Goates, J.; Crawford, M. K. *J. Chem. Thermodyn.* **2004**, *36*, 349.
(5) (a) Yan, C.; Singh, N.; Lee, P. S. *Appl. Phys. Lett.* **2010**, *96*, 053108. (b) Yan, C.; Lee, P. S. *J. Phys. Chem. C* **2010**, *114*, 265.
(6) Liu, Z.; Jing, X.; Wang, L. *J. Electrochem. Soc.* **2007**, *154*, H500.
(7) (a) Ma, B.; Wen, F.; Jiang, H.; Yang, J.; Ying, P.; Li, C. *Catal. Lett.* **2010**, *134*, 78. (b) Sato, J.; Kobayashi, H.; Ikarashi, K.; Saito, N.; Nishiyama, H.; Inoue, Y. *J. Phys. Chem. B* **2004**, *108*, 4369. (c) Huang, J. H.; Wang, X. C.; Hou, Y. D.; Chen, X. F.; Wu, L.; Fu, X. Z. *Environ. Sci. Technol.* **2008**, *42*, 7387. (d) Huang, J.; Ding, K.; Hou, Y.; Wang, X.; Fu, X. *ChemSusChem* **2008**, *1*, 1011.
(8) Tsai, M. Y.; Yu, C. Y.; Wang, C. C.; Perng, T. P. *Cryst. Growth Des.* **2008**, *8*, 2264.
(9) For reviews, see: (a) Yao, W. T. *Adv. Funct. Mater.* **2008**, *18*, 3357. (b) Yao, H. B.; Gao, M. R.; Yu, S. H. *Nanoscale* **2010**, *2*, 323. (c) Li, J.; Chen, Z.; Wang, R. J.; Proserpio, D. M. *Coord. Chem. Rev.* **1999**, *190*−*192*, 707. (d) Hagrman, P. J.; Hagrman, D.; Zubieta, J. *Angew. Chem., Int. Ed.* **1999**, *38*, 2638.
(10) Gao, Q. S.; Chen, P.; Zhang, Y. H.; Tang, Y. *Adv. Mater.* **2008**, *20*, 1837.
(11) Li, Y. D.; Liao, H. W.; Ding, Y.; Fan, Y.; Zhang, Y.; Qian, Y. T. *Inorg. Chem.* **1999**, *38*, 1382.
(12) (a) Lu, Q. Y.; Gao, F. *Nano Lett.* **2002**, *2*, 725. (b) Yang, J.; Xue, C.; Yu, S. H.; Zeng, J. H.; Qian, Y. T. *Angew. Chem., Int. Ed.* **2002**, *41*, 4697.
(13) Roy, S. C.; Varghese, O. K.; Paulose, M.; Grimes, C. A. *ACS Nano* **2010**, *4*, 1259.

JA1068596